Corrosion Science 198 (2022) 110134

Contents lists available at ScienceDirect

Corrosion Science

journal homepage: www.elsevier.com/locate/corsci

Formation and oxidation behavior of refractory high-entropy silicide (NbMoTaW)Si_2 coating

Juan Kuang [a], Ping Zhang [b], Qianqian Wang [a,c], Zhenfeng Hu [d], Xiubing Liang [d], Baolong Shen [a,*]

[a] School of Materials Science and Engineering, Jiangsu Key Laboratory for Advanced Metallic Materials, Southeast University, Nanjing, Jiangsu 211189, China
[b] School of Material Science and Engineering, China University of Mining and Technology, Xuzhou, Jiangsu 221116, China
[c] School of Materials Science and Engineering, Jiangsu Key Laboratory of Advanced Structural Materials and Application Technology, Nanjing Institute of Technology, Nanjing, Jiangsu 211167, China
[d] Defense Innovation Institute, Academy of Military Science, Beijing 100071, China

ARTICLE INFO

Keywords:
Refractory high entropy alloy
High entropy silicide
Oxidation behavior

ABSTRACT

A single high-entropy silicide (NbMoTaW)Si_2 coating was prepared on NbMoTaW refractory alloy by a halide-activated pack cementation process. The formation mechanism and growth kinetics of the (NbMoTaW)Si_2 coatings were analysed. The oxidation behavior of the (NbMoTaW)Si_2 coatings was investigated at 1300 ℃ for 24 h in air. The results showed that the high entropy effect and sluggish effect of the high-entropy NbMoTaW alloy makes it form a single-phase silicide (NbMoTaW)Si_2 during the Si diffusion growth process. The lattice distortion effect of substrate provides a channel for the diffusion of Si to accelerate its diffusion rate. The (NbMoTaW)Si_2 coating effectively protects the NbMoTaW alloy from oxidation at 1300 ℃. The oxidation resistance of the coating is attributed to the preferential oxidation of Si to produce a dense continuous SiO_2 scale and the precipitation of WSi_2 to suppress the interdiffusion of the silicide layer and the alloy substrate.

1. Introduction

High entropy alloys (HEAs), also named multi-principal element alloys (MPEAs), are a new type of structural material consisting of multiple elements (at least three) at equiatomic or near-equiatomic concentrations [1,2]. There are four core effects in HEAs: the high entropy effect, the lattice distortion effect, the sluggish diffusion effect and the cocktail effect [3,4]. Refractory high-entropy alloys (RHEAs), based on refractory metal elements (such as W, Ta, Re, Mo, Nb, Hf), are potential high temperature structural materials to meet the aggressive demand of raising the operation temperature (> 1000 °C) in next-generation jet engines and nuclear reactors due to their high melting point, high-temperature strength, high hardness and excellent phase stability at high temperatures [5–7]. Equiatomic NbMoTaW and VNbMoTaW RHEAs were reported for the first time by Senkov et al. in 2010 [8,9]. The NbMoTaW and VNbMoTaW alloys show potential use above 1200 ℃. Strong resistance to strain softening is observed in NbMoTaW, which retains steady state flow to 1600 ℃, but MoNbTaVW shows strain softening above 1200 ℃. The NbMoTaW RHEA had a stable single-phase BCC solid solution structure at 1400 ℃ and maintained high strength at high temperature (506 MPa at 1200 ℃ and 405 MPa at 1600 ℃).

However, RHEAs will undergo catastrophic oxidation in a high-temperature aerobic environment, due to the rapid formation of volatile oxides (MoO_3, WO_3, VO_3 etc.) and easily peeling oxides (Nb_2O_5, Ta_2O_5) that do not have high-temperature protection capabilities. The poor oxidation resistance of RHEAs at high-temperature becomes a key limitation for their wide application [10]. It is urgent to improve the oxidation resistance of NbMoTaW RHEA above 1200 ℃.

The addition of antioxidant alloy elements (such as Al, Cr, Si) is one of the methods to improve the oxidation resistance of RHEAs, but it inevitably reduces the high temperature mechanical properties of alloys [11]. Applying protective coatings on the surface is the easiest and most efficient approach to improve substrate oxidation resistance. Among antioxidant coatings, silicide coatings with high melting points, good thermal stability, and good self-healing ability have been widely used to protect refractory metals. The dense SiO_2 layer formed on the surface of the coating during oxidation can hinder the inward diffusion of oxygen [12]. However, there is still less work to prepare coatings on the surface of refractory high-entropy alloys.

* Corresponding author at: School of Materials Science and Engineering, Jiangsu Key Laboratory for Advanced Metallic Materials, Southeast University, Nanjing, Jiangsu 211189, China.
E-mail address: blshen@seu.edu.cn (B. Shen).

https://doi.org/10.1016/j.corsci.2022.110134
Received 14 November 2021; Received in revised form 23 January 2022; Accepted 27 January 2022
Available online 1 February 2022

Han et al. [13] prepared a Si-20Cr-20Fe coating on MoNbTaTiW RHEA by a fused slurry method. The silicide coating could effectively prevent the oxidation of the MoNbTaTiW RHEA at 1000 ℃ and 1300 ℃ for 1 h. However, the silicide coating prepared by the fused slurry method had a large number of pores, which affected the oxidation resistance of the coating. The halide activated pack cementation (HAPC) technique, an in-situ chemical vapor deposition technology, is one of the most widely used diffusion coating processes for applying protective silicide coatings on refractory alloys [14–16]. Yang et al. [17] studied Si/Al pack cementation coatings on MoNbTaVW alloys to improve their oxidation resistance after flame tests at 1350 ℃ for 20 min. It had a coating layer of approximately 80 μm with a sequence of Si-rich layer (silicide)/interdiffusion layer/Al-rich layer (aluminide)/Al diffusion layer, presenting a complex phase rather than a single-phase. The diffusion mechanism in the process of pack cementation needs to be further studied. The long-term oxidation of the protective coating on refractory high-entropy alloys above 1300 ℃ remains to be studied.

In this work, silicide coatings with a single high-entropy silicide (NbMoTaW)Si_2 phase were prepared on NbMoTaW RHEA by the pack cementation method. The formation mechanism and growth kinetics of the (NbMoTaW)Si_2 coatings were dissected. In order to dissect the substrate effects of NbMoTaW RHEA, the growth of coatings fabricated on pure metals (pure Nb, pure Mo, pure Ta, and pure W) by the same process was also studied. The oxidation behavior of the (NbMoTaW)Si_2 coatings at 1300 ℃ was investigated, and the formation of the oxide scale and microstructure evolution of the coatings were discussed.

2. Materials and methods

The NbMoTaW alloy samples were prepared using high purity (> 99.9%) elemental metals through arc-melting. During arc melting, the button ingots were flipped and re-melted at least five times to improve chemical homogeneity. Specimens with dimensions of 6 mm × 6 mm× 3 mm were cut from the ingots and polished with a series of SiC papers up to grit 1500#. The edges of the specimens were round to suppress the formation of cracks at sharp corners. The specimens were then ultrasonically cleaned in alcohol and deionized water, and dried under cold air.

The (NbMoTaW)Si_2 coating was fabricated by the halide-activated pack cementation method. The pack mixture used for the process was composed of 30 wt% Si, 5 wt% NaF and 65 wt% Al_2O_3. The substrate samples were packed and sealed in alumina crucibles with a powder mixture. After that, the packed crucible was loaded in a high temperature and high vacuum furnace. The furnace was heated to the deposition temperature at a rate of 10 ℃/min in an Ar protective atmosphere. The pack cementation process was carried out at different temperatures of 1373 K, 1473 K, and 1573 K for different holding times of 0, 0.5, 1, 1.5, 2, 3, 4, and 5 h to study the structural evolution of the coatings. After reaching the holding time, the coating specimens were cooled to room temperature in the furnace. In order to dissect the substrate effects of high entropy NbMoTaW alloy, the growth of coatings fabricated on metals (pure Mo, pure Nb, pure Ta and pure W) by the same HAPC process was also studied.

The oxidation tests of the coating and alloy specimens were conducted isothermally in an electric furnace at 1300 ℃ for different time in air. The specimens were removed immediately from the furnace when the set time was reached, and cooled in air. The mass changes of the specimens after oxidation tests were measured using a high-precision electronic balance with an accuracy of 10^{-5} g. Three measurements for each specimen were conducted and the average value was obtained.

The surface morphology of the coatings was characterized by scanning electron microscopy (SEM, FEI Sirion 200, USA) with energy dispersive spectrometry (EDS). The microscopic ruler of an optical microscope was used to measure the thickness of the coating at different positions on the two opposite sides of the coatings. The phase analysis was characterized by X-ray diffraction (XRD) with Cu Kα (Rigaku D/max 2500, Japan). The crystal structure of the coatings was characterized using a high-resolution transmission electron microscope (HRTEM, Talos F200X, USA). Composition analysis of the cross section of the coating after oxidation was operated on an electron-probe microanalysis (EPMA, JEOL JXA-8230, Japan).

3. Results and discussion

3.1. Coating characterizations

Fig. 1 shows the X-ray diffraction analysis spectrum of the surface of the coatings on the NbMoTaW alloy. The measured interplanar distance and relative intensity of diffraction lines were compared with standard JCPDS cards for phase analysis through the software Jade 6. For the coatings formed at different preparation temperatures and holding times, the XRD results are basically the same, which means that the composition of the prepared coating is not influenced by temperature or holding time. The characteristic diffraction peaks correspond to single phase hexagonal C40-MSi_2 crystal structure with space group $P6_222$ (180) rather than pure $NbSi_2$, $MoSi_2$, $TaSi_2$, and WSi_2 phases (e.g., the peak position for (111) peak of $NbSi_2$, $MoSi_2$, $TaSi_2$, WSi_2 and the sample prepared in this work are 39.947°, 41.603°,40.096°, 41.225° and 40.662°, respectively), confirming the presence of (NbMoTaW)Si_2 phase. The estimated lattice parameters of the silicide coating are 4.711 Å for a and 6.545 Å for c. The crystal structure of the formed silicide is consistent with refractory high-entropy silicides, such as ($Mo_{0.2}Nb_{0.2}Ta_{0.2}Ti_{0.2}W_{0.2}$)$Si_2$, ($Mo_{0.2}W_{0.2}Cr_{0.2}Ta_{0.2}Nb_{0.2}$)$Si_2$, (CrMoTaVNb)$Si_2$, and (CrMoTa)$Si_2$ reported in previous studies [18–20]. The NbMoTaW RHEA with high entropy effect and sluggish diffusion effect maintains a solid solution structure to form a single-phase silicide during the growth of the coating. It also introduces a large number of stable vacancies with a high migration energy barrier to form high entropy, resulting in a slow diffusion effect to hinder the diffusion of metal cations [21]. The high entropy silicide (NbMoTaW)Si_2 keeps the metal elements to replace each other and share the cation position, while Si occupies the anion position. It has been proposed that severe lattice distortion would exist in (NbMoTaW)Si_2 owing to the intrinsic atomic disorder of metal elements.

Typical cross-sectional BSE images of coatings formed at different deposition temperatures and holding times are presented in Fig. 2. The silicide coatings formed under all parameters are a single layer that is relatively uniform, dense, continuous, and metallurgically combined with the substrate, which shows good interfacial bonding. In the pack cementation experiment, the samples were heated to 1473 K with the furnace and then cooled to room temperature with the furnace at a certain heating/cooling rate. As a result, the thickness of the prepared coating with a holding time of 0 h reaches 26 μm. The morphology and structure of the coating layer are basically the same, but the thickness of the coating gradually increases with an increase in the holding time or the deposition temperature. The continuous penetration of Si continuously reacts with the substrate to form the (NbMoTaW)Si_2 coating. Clearly, cracks appear in the coating due to the increased internal stress caused by the growth of the coating when the holding time is too long at 1473 K. Furthermore, the cracks and peeling of the coating are devastating when the preparation temperature is 1573 K.

To verify the distribution of Nb, Mo, Ta, W and Si, elemental maps of the prepared coating at 1473 K for 1.5 h are shown in Fig. 3a. The result shows that the thickness of Si inward diffusion reaches 75 μm, and the distribution of Si in the coating is uniform, which is consistent with the single-phase structure of the coating mentioned above. In addition, Nb, Mo, Ta and W in the coating can be observed to maintain the same distribution as the alloy substrate. The EDS analysis results shown in Table 1 reveal the chemical compositions of different areas in the coating and alloy substrate. From the outer layer to the inner layer of the coating, the content of all elements is basically the same. The ratio of the atomic percent of Si to the sum of that of Nb, Mo, Ta and W is 2:1. Combined with the XRD results in Fig. 1, it can be concluded that the

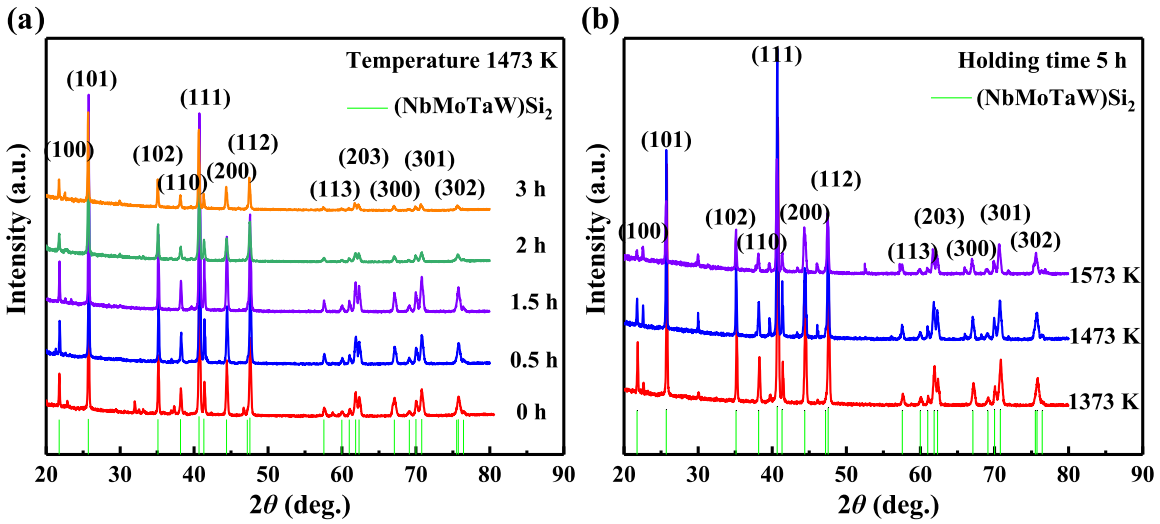

Fig. 1. XRD patterns for the surfaces of the silicide coatings formed at: (a) different preparation temperatures for 5 h; (b) different holding times at 1473 K.

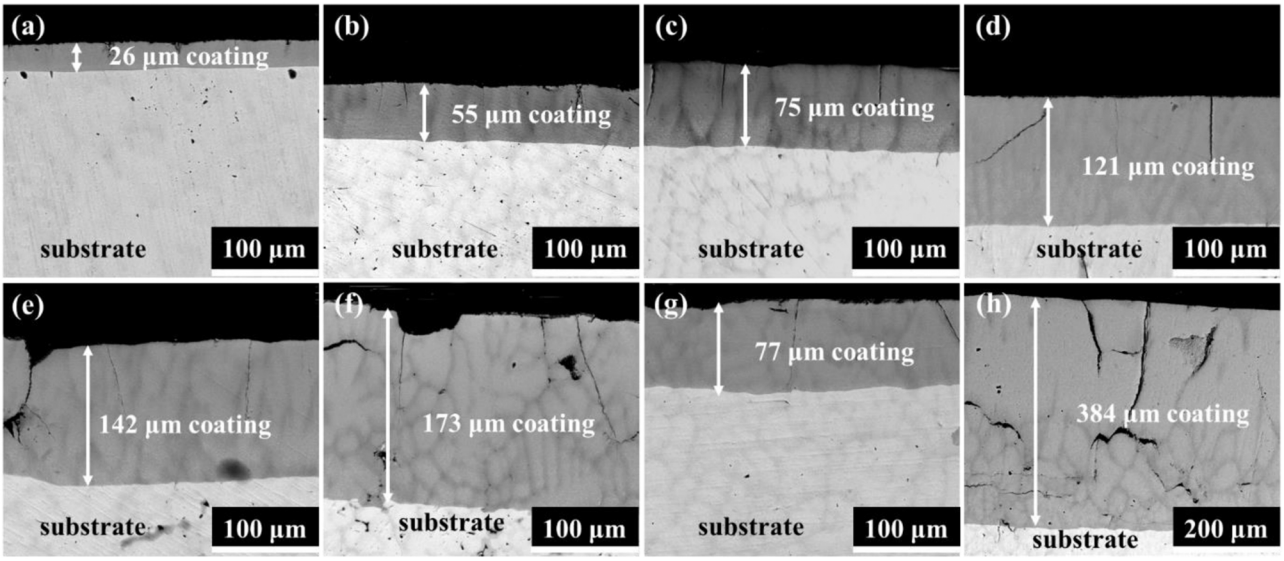

Fig. 2. Cross-sectional SEM micrographs of coatings after pack cementation at 1473 K for (a) 0 h; (b) 0.5 h; (c) 1.5 h; (d) 2 h; (e) 3 h; (f) 5 h; (g) 1373 K for 5 h; (h) 1573 K for 5 h.

high entropy (NbMoTaW)Si_2 coating is formed by the following reaction equation.

$$NbMoTaW + 2Si \rightarrow \quad (NbMoTaW)Si_2 \tag{1}$$

TEM images and elemental maps of the coating powder are shown in Fig. 3b. The EDS analysis results reveal that it is (NbMoTaW)Si_2 and there is no difference in the chemical compositions of all areas. Fig. 3c shows SAED patterns of area C. The two sides of the parallelogram for phase C possess D-spacings of 3.996 Å and 2.193 Å, which are determined to be the (1 0 0) and ($\bar{1}$ 2 $\bar{1}$) reflections of (NbMoTaW)Si_2 with a $P6_222$ structure. These results are in good agreement with the XRD (Fig. 1) and EDS results.

3.2. Coating growth kinetics

The thermodynamic factors in reaction diffusion should be first considered. Fig. 4a shows the corresponding Gibbs free energy variation of the formation of MSi_2 (M represents Nb, Mo, Ta and W) as a function of temperature, based on HSC 6.0 software [22]. The Gibbs free energy of all metal disilicides is negative from 373 K to 1573 K, indicating that these disilicides can be formed spontaneously during the HAPC process from a thermodynamic point of view. However, thermodynamic factors can only reflect the directionality of the reaction, and the specific coating process and growth rate depend on kinetic factors.

The thickness of the coatings formed on the NbMoTaW alloy, pure Nb, pure Mo, pure Ta and pure W at different temperatures for different holding times was measured, as shown in Fig. 4(b–d). The coating on the NbMoTaW alloy is perpetually thicker than that of the coatings on pure metals. In the pack cementation process, the formation of the silicide layer involves three indispensable processes. Firstly, the activator (NaF) reacts with Si and forms a number of vapor silicon fluoride species SiF_x ($1 \leq x \leq 4$) such as SiF_4, SiF_3, SiF_2, and SiF via Eq. (2). Driven by the chemical potential gradient, these SiF_x species diffuse to the surface of the sample through the gaps between the particles of the encapsulated powder. Secondly, decomposition and reduction reactions of silicon fluoride species occur, resulting in the formation of active [Si] at the atomic scale (Eq. (3)) [23].

$$\mathrm{Si(s)} + xNaF(s) \rightarrow SiF_x(g) + xNa \tag{2}$$

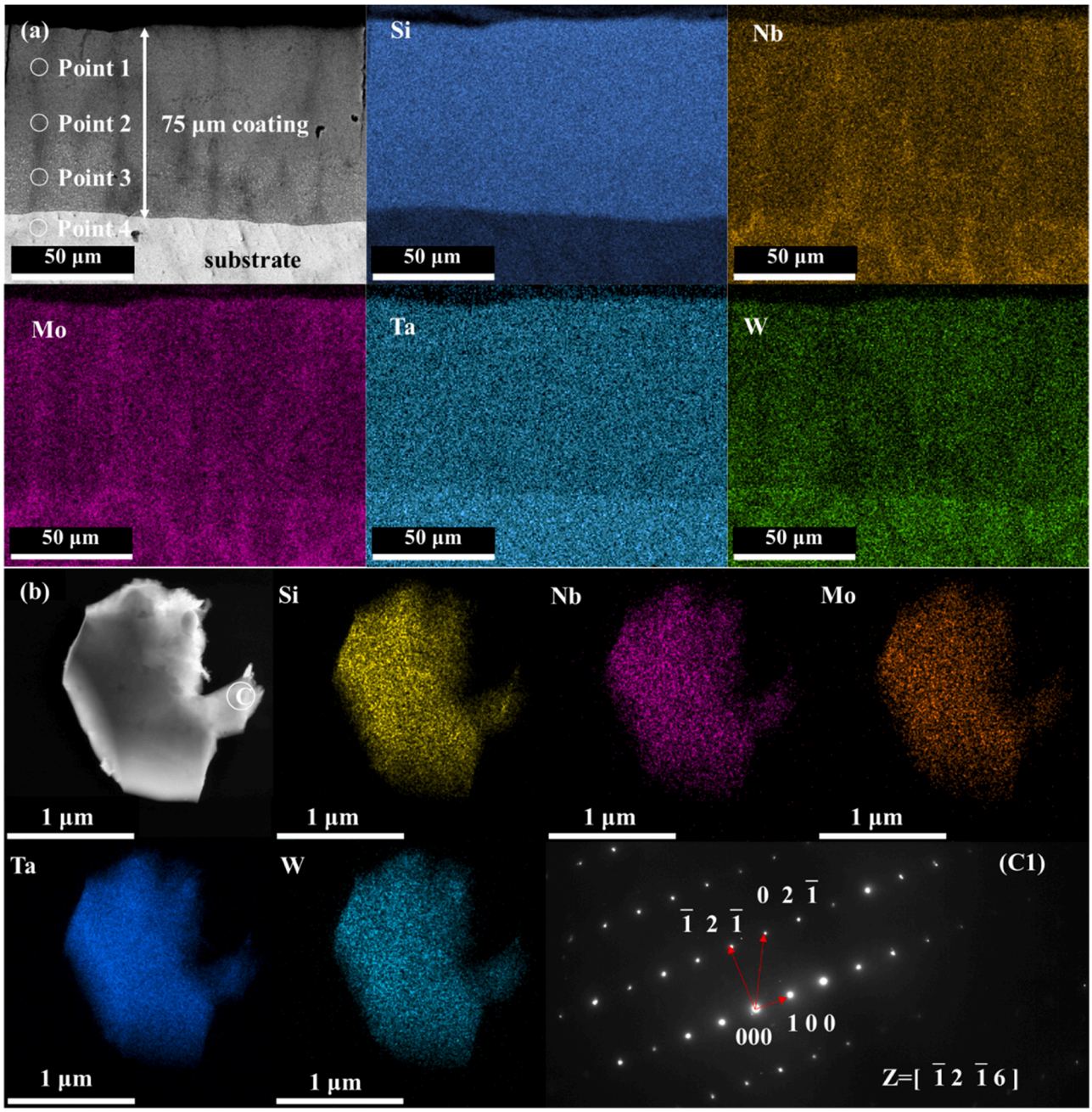

Fig. 3. (a) Elemental mapping of coating formed at 1473 K for 1.5 h; (b) TEM of the coating.

Table 1
EDS composition analysis of different areas of the coating formed at 1473 K for 1.5 h (corresponding with Fig. 2a).

Point	Atomic percent %					
	Si	Nb	Mo	Ta	W	Total
1	68.4	7.8	7.6	7.7	8.5	100.0
2	69.2	7.0	7.1	7.9	8.8	100.0
3	63.3	8.9	8.9	9.4	9.5	100.0
4	–	21.2	22.7	29.2	26.9	100.0

$$(x+1)SiF_x(g) \rightarrow xSiF_{x+1}(g) + [Si] \quad (3)$$

Lastly, atomic diffusion reaction between active Si atoms and the substrate takes place to generate the silicide layer on the surface [12]. Thus, the growth of the silicide coating is dominated by the inward diffusion of Si [24]. The Wagner scale theory could describe the parabolic growth rate of the coating as follows:

$$y^2 = Kt + b \quad (4)$$

y is the thickness of the coating (m); t is the holding time (s); K is the diffusion coefficient (m^2/s).

The relationship curve between the square of the silicide coating thickness of alloy and pure metals and the holding time at different preparation temperatures was drawn, as shown in Fig. 5(a–c). Fig. 5 shows the growth kinetics of silicide coating in the NbMoTaW RHEA, as well as in the metals (pure Mo, pure Nb, pure Ta and pure W), which also reflects the diffusion of Si in alloys and pure metals. The square of the coating thickness has a linear relationship with the holding time, and the diffusion coefficients of Si in the NbMoTaW alloy and pure metals can be calculated according to the slope of the fitting line, which are listed in

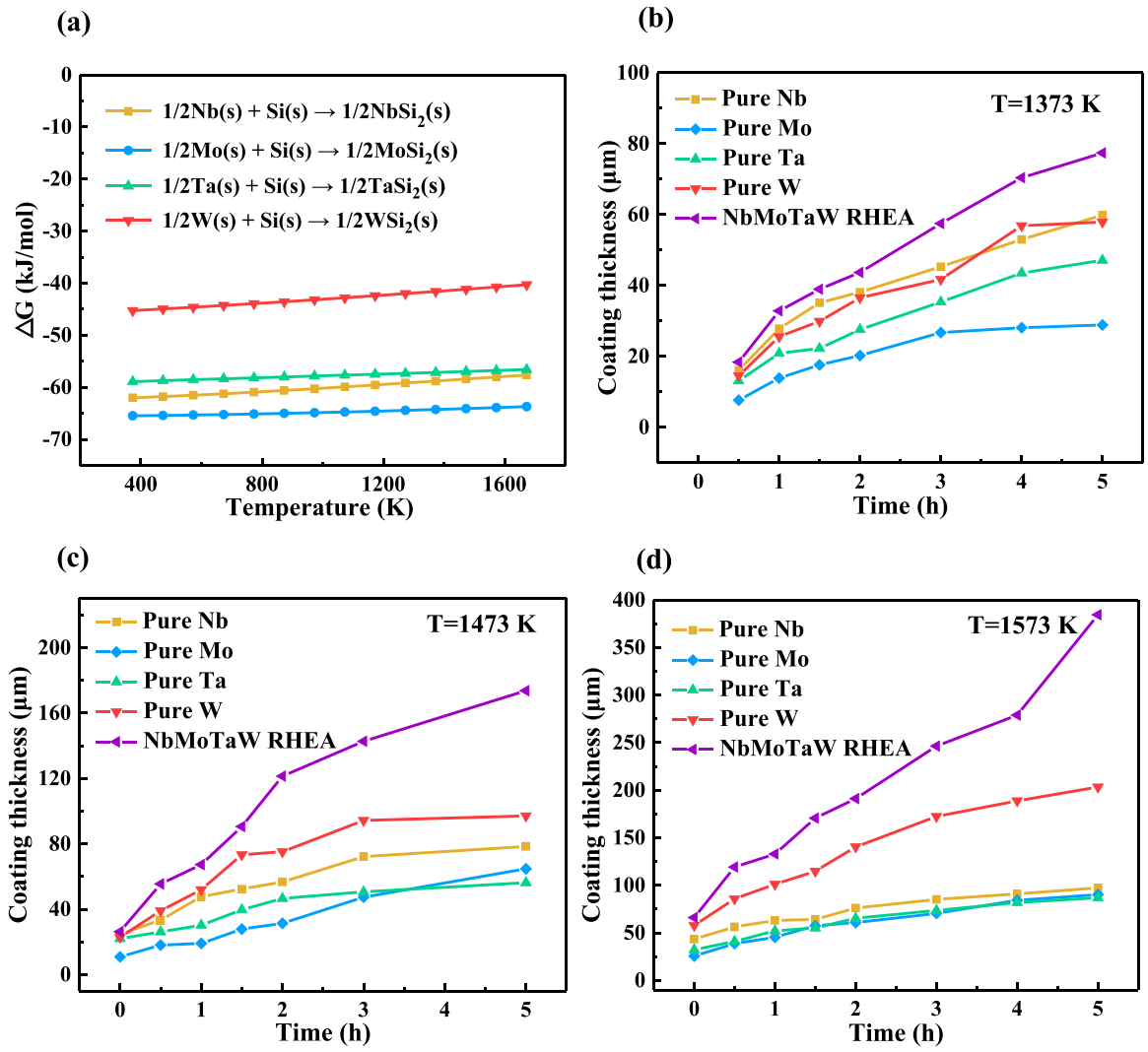

Fig. 4. (a) Temperature dependence of the Gibbs free energy variation of formation of MSi_2, M represents for Nb, Mo, Ta, W; (b-d) Coating thickness of Si diffusion in RHEA alloy and pure metals at different preparation temperatures:(b) 1373 K, (c) 1473 K, (d) 1573 K.

Table 2. For the same substance, the diffusion coefficient of Si increases with increasing preparation temperature. Generally, the effects of temperature increase include: increasing the thermal activation energy of diffusing atoms, increasing the probability of surpassing the barrier, and increasing the concentration of vacancies, which make the atoms more prone to migration and diffusion. At the same preparation temperature, the diffusion coefficient of Si in the NbMoTaW alloy is always greater than that of the elemental metal. For high entropy NbMoTaW alloy, each atom is randomly distributed in the crystal lattice. The radii and chemical bonds of different metal atoms are quite different, and the surrounding environment and occupancy of each atom are different, which makes the NbMoTaW alloy crystal lattice have larger lattice distortion and defects than pure metals. It is conducive to the migration of diffused atoms along the distortion and defects zone from high concentration to low concentration at high temperature, which speeds up diffusion. The lattice distortion effect of the NbMoTaW alloy provides a channel for the diffusion of Si, thereby accelerating its diffusion rate.

The relationship between the diffusion coefficient, activation energy, and the process temperature can be expressed according to the Arrhenius formula:

$$K = K_0 exp(-\frac{Q}{RT}) \quad (5)$$

Q is the activation energy of diffusion (kJ/mol); R is the gas constant, 8.314 J/(mol·K), T is the temperature (K).

Taking the natural logarithm of Eq. (5), Eq. (6) can be derived as follows:

$$InK = InK_0 - \frac{Q}{RT} \quad (6)$$

From the diffusion coefficient of Si in alloys and pure metals in Table 2, the relationship between ln$K$ and $1/T$ can be drawn as shown in Fig. 5d, which shows the activation energy in the process of pack cementation. The linear slope -Q/R after linear fitting is obtained, and then the calculation of the diffusion activation energy(Q) of Si in the NbMoTaW alloy and pure metals is shown in Table 3. The diffusion activation energy of Si in the NbMoTaW alloy is the largest, indicating that it has the strongest dependence on the preparation temperature.

3.3. Oxidation behavior

The silicide coating specimens fabricated at 1473 K for 1.5 h were oxidized at 1300 ℃ up to 24 h in static air to estimate the oxidation resistance of the (NbMoTaW)Si_2 coating. For comparison, the uncoated NbMoTaW alloys were also oxidized at 1300 ℃ up to 30 min Fig. 6 presents their oxidation gravimetric curves. The bare alloy exhibits a relatively poor oxidation resistance because it follows the law of linear weight gain and its mass gain reaches 65 mg/cm^2 after exposure for

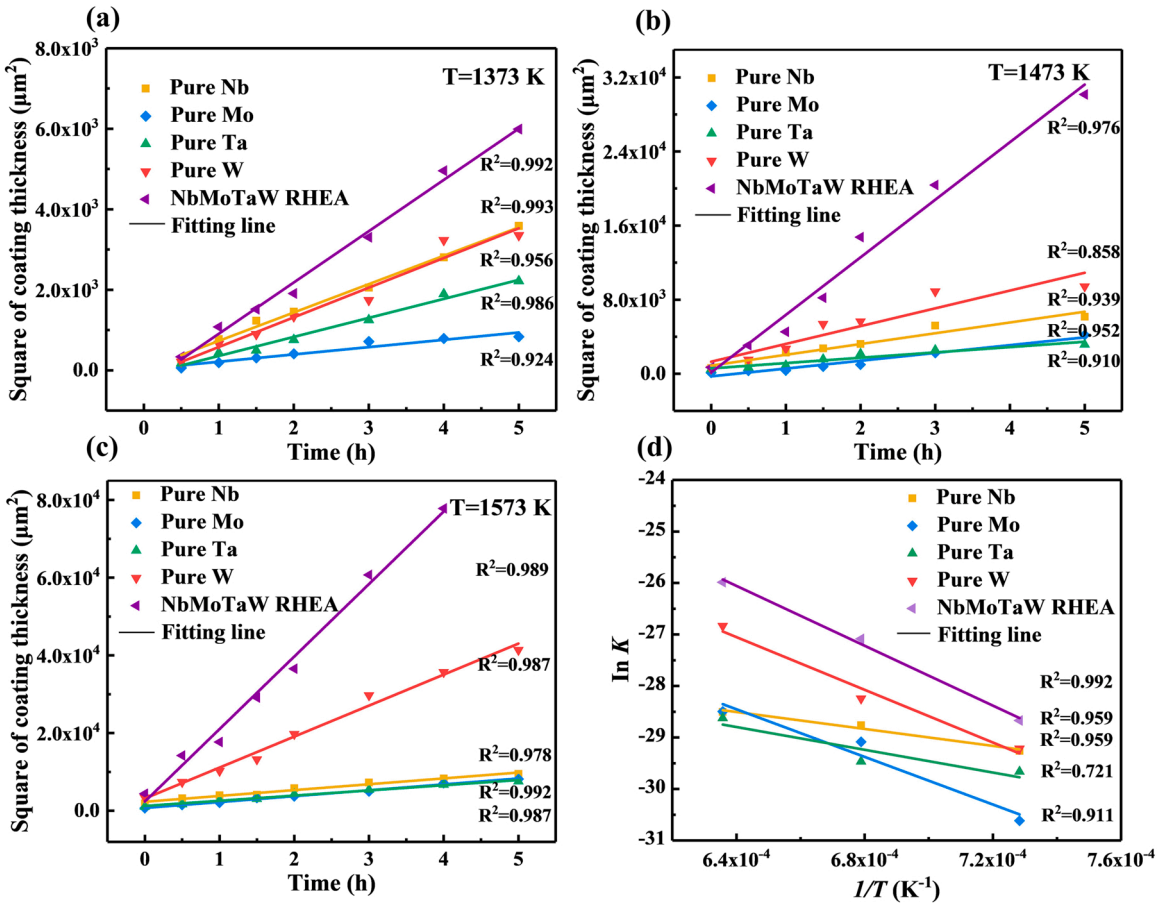

Fig. 5. Reaction kinetics curves of Si diffusion in RHEA alloy and pure metals at different holding temperatures:(a) 1373 K; (b) 1473 K; (c) 1573 K; (d) Calculation chart of activation energy in the process of pack cementation.

Table 2
Diffusion coefficient value of Si in pure metals and NbMoTaW RHEA fitted and calculated from Fig. 5(a–c).

Diffusion coefficient K (m^2/s)	1373 K	1473 K	1573 K
Pure Nb	1.959×10^{-13}	3.231×10^{-13}	4.179×10^{-13}
Pure Mo	5.042×10^{-14}	2.340×10^{-13}	4.212×10^{-13}
Pure Ta	1.312×10^{-13}	1.599×10^{-13}	3.712×10^{-13}
Pure W	2.047×10^{-13}	5.419×10^{-13}	2.216×10^{-12}
NbMoTaW RHEA	3.539×10^{-13}	1.727×10^{-12}	5.186×10^{-12}

Table 3
Diffusion activation energy values of Si in pure metals and NbMoTaW RHEA fitted and calculated from Fig. 5d.

Diffusion activation energy	Pure Nb	Pure Mo	Pure Ta	Pure W	NbMoTaW RHEA
$-Q/R$	-8228.22	-23118.43	-11056.34	-25575.88	-29065.16
Q (kJ/mol)	68.409	192.207	91.922	212.38	241.65

30 min. In contrast, the oxidation mass gain of the coating specimen exhibits a parabolic increase and it is approximately 32 mg/cm^2 after oxidation for 24 h.

The XRD patterns on the surface of the NbMoTaW alloy and (NbMoTaW)Si_2 coating specimen after oxidation for different times are shown in Fig. 7. The diffraction peaks of the unique BCC structure of the original substrate NbMoTaW can no longer be seen from the Fig. 7a, indicating that the alloy substrate has formed a thicker oxide layer on the surface after being oxidized for 5 min. With the extension of

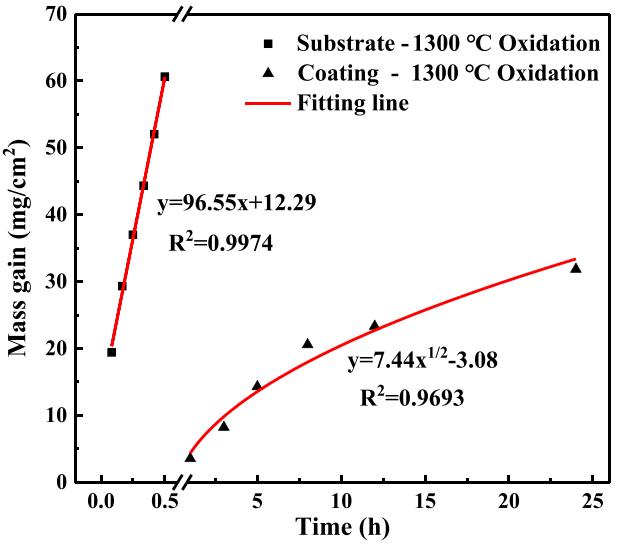

Fig. 6. Oxidation kinetics curves of the substrate and coating: (a) NbMoTaW alloy at 1300 ℃ for 30 min; (b) the (NbMoTaW)Si_2 coating spcimen at 1300 ℃ for 24 h.

oxidation time, the oxidation products of NbMoTaW alloy are basically the same, mainly Nb_2O_5 (PDF: 19-0862), Ta_2O_5 (PDF: 35-1193), and WO_3 (PDF: 05-0388). In addition, WO_3 easily reacts with Ta_2O_5 to form complex oxides $Ta_{16}W_{18}O_{94}$ (PDF: 29-1323) at high-temperature. Regardless of the initial stage or the later stage of oxidation, no Mo-

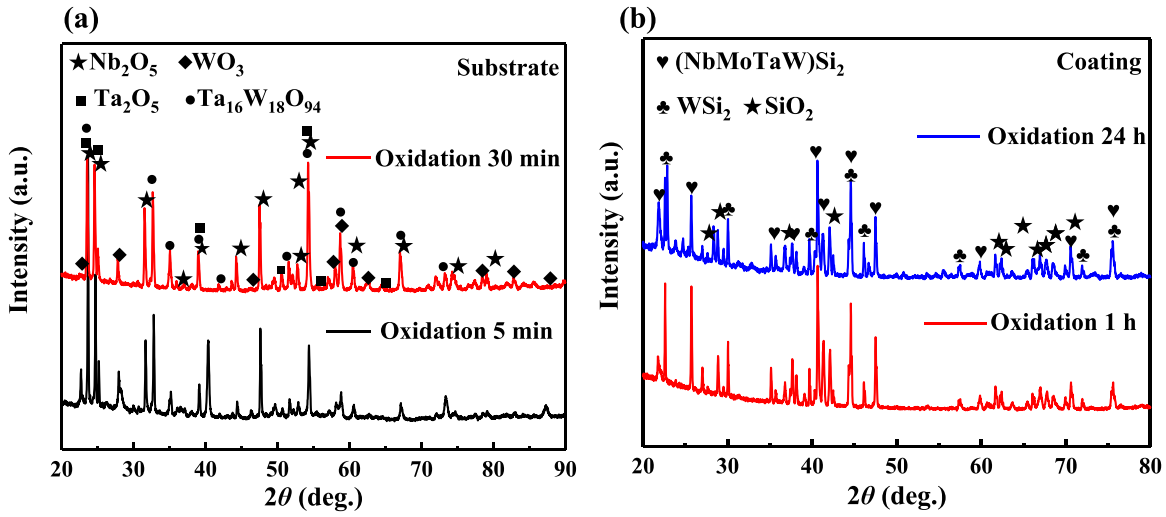

Fig. 7. XRD patterns of the NbMoTaW alloy (a) and (NbMoTaW)Si_2 coating spcimen (b) after oxidation at 1300 ℃ for different times.

containing oxide was found in the oxide layer in the XRD analysis, which is mainly because MoO_3 is volatile at 1300 ℃. However, for the (NbMoTaW)Si_2 coating specimen (as shown in Fig. 7b), strong characteristic peaks of the original silicide coating are detected on the surface. It indicates that the oxide layer on the surface of the (NbMoTaW)Si_2 coating specimen is still thin even after oxidation for 24 h. In addition to the characteristic peak of (NbMoTaW)Si_2, the characteristic peak of WSi_2 (PDF: 11-0195) also appears. This result indicates that the high entropy silicide (NbMoTaW)Si_2 segregates after a high-temperature oxidation, leading to the precipitation of WSi_2 with tetragonal structure and space group of I4-mmm(139). The oxidation product of the (NbMoTaW)Si_2 coating is only SiO_2 and there are no base metal oxides, which indicates that the outward diffusion oxidation of metal elements was inhibited.

Fig. 8 shows the surface morphology of the NbMoTaW alloy and (NbMoTaW)Si_2 coating specimen after oxidation at 1300 ℃ for 30 min and 24 h, respectively. Judging from the macrophotographs after oxidation (in the inserted figure in Fig. 8a), the edges and corners of the NbMoTaW alloy are severely split. The micromorphology presents the disorderly growth of small and dense stick-shaped oxidation products. The volume expansion of oxidation products would cause a large interface stress, since the Pilling-Bedworth rate (PBR) of Nb_2O_5, Ta_2O_5, WO_3 exceeds 1.5, which would even tear the adhesive surface oxide scale, providing a channel for oxygen internal diffusion.

In comparison, the oxidation resistance of the (NbMoTaW)Si_2 coating specimen is significantly improved, which maintains its original shape without severe cracks after oxidation for 24 h. The surface micromorphology shows that a relatively flat and smooth surface can be obtained. Combined with the XRD results in Fig. 7b, the surface is covered by successive and uniform glassy SiO_2, which is related to the oxidation of the (NbMoTaW)Si_2 coating. The formation of oxide films during high temperature oxidation is closely related to the Gibbs free

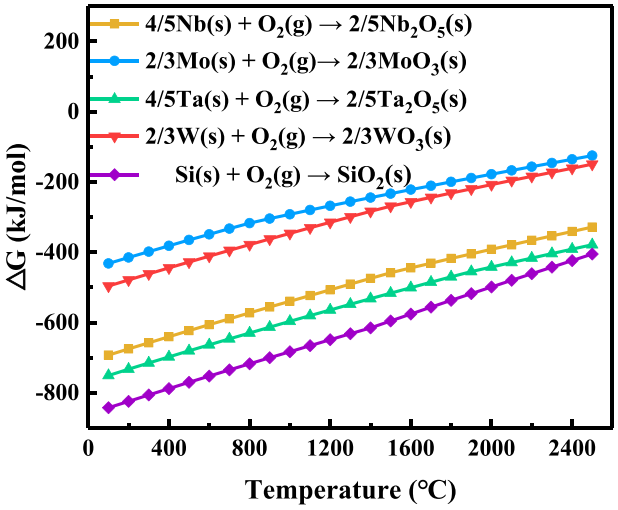

Fig. 9. Temperature dependence of the Gibbs free energy of oxides.

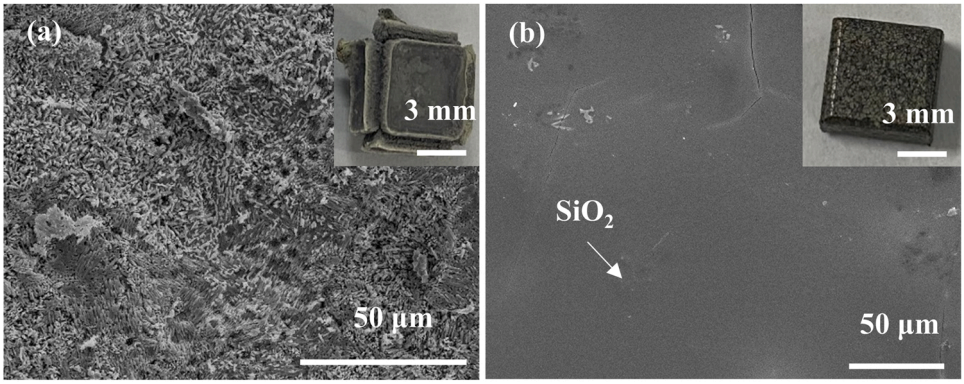

Fig. 8. Surface SEM and cross-section BSE images of (a) the NbMoTaW alloy after oxidation at 1300 ℃ for 30 min; (b)(NbMoTaW)Si_2 coating specimen after oxidation at 1300 ℃ for 24 h.

energy. Generally, oxides with lower Gibbs free energy are preferentially formed during oxidation. Fig. 9 shows the Gibbs free energy of the oxides. The Gibbs free energy of SiO_2 is lowest, indicating that Si is oxidized preferentially in $(NbMoTaW)Si_2$.to form SiO_2 with good oxidation resistance. Preferential oxidation of Si also occurs at the cracks of the coating during the oxidation process. The formation of glassy SiO_2 scale can play a role in healing coating cracks [25].

In addition, Fig. 10(a, b) shows a cross-sectional view of the $(NbMoTaW)Si_2$ coating specimen after oxidation for 1 h and 24 h, which are both composed of three layers. According to the EDS and XRD results (Table 4 and Fig. 7b), the main components of the oxide layer, silicide coating layer and diffusion layer are SiO_2, $(NbMoTaW)Si_2/WSi_2$ and $(NbMoTaW)_5Si_3$, respectively. The $(NbMoTaW)_5Si_3$ layer is formed by interdiffusion between the $(NbMoTaW)Si_2$ coating and the NbMoTaW alloy substrate. Specifically, Si from the coating layer diffuses inward and (Nb, Mo, Ta, W) from the substrate diffuses outward. The inward diffusion of Si has a greater influence on the thickness of the $(NbMoTaW)_5Si_3$ layer than the outward diffusion of metals [24]. The thicknesses of the oxide layer, silicide coating layer and diffusion layer in the initial oxidation stage are 5 μm, 85 μm and 5 μm, respectively. With the extension of the oxidation time, the thickness of the oxide layer changes little, reaching 8 μm after 24 h, while the thickness of the diffusion layer increases significantly to 15 μm. It indicates that the preferentially formed SiO_2 oxide layer is continuous and dense on the surface, which hinders the inward diffusion of oxygen and the external diffusion of the silicide $(NbMoTaW)Si_2$ during the oxidation process. As a result, the Si in the $(NbMoTaW)Si_2$ coating diffuses more into the substrate, and the formed $(NbMoTaW)_5Si_3$ layer thickens more.

In order to further analyze the element distributions of the silicide coating after oxidation, EPMA mapping is performed on the cross-sectional scale as shown in Fig. 10b. It can be seen clearly that oxygen is mainly dispersed in the oxide scale, while almost no Nb, Mo, Ta, W are found in the scale, suggesting that the scale can effectively prevent the mobility of oxygen and the external diffusion of alloy elements. A large number of white particles precipitated in the silicide coating layer, which corresponds to the WSi_2-rich phase. According to the XRD results, it can be inferred that the precipitation of WSi_2 with a tetragonal structure occurs during oxidation. WSi_2 has been considered to be a good diffusion barrier against Si and metallic atoms [26]. The high melting point and improved mechanical properties of WSi_2 are beneficial for improving the comprehensive performance of the silicide coating. Dayananda pointed out that the transition rate of WSi_2 to W_5Si_3 is on average four times slower than that of $MoSi_2$ to Mo_5Si_3 [27]. The precipitation of WSi_2 can slow down the diffusion of Si into the alloy substrate, thereby providing sufficient Si for the formation of SiO_2.

To better understand the oxidation process of the high-entropy silicide coating, a schematic diagram of the oxidation process of the $(NbMoTaW)Si_2$ coating at 1300 ℃ is shown in Fig. 11. The protective SiO_2 forms primarily on the surfaces of the coating at the initial stage attributed to the selective oxidation of Si in the $(NbMoTaW)Si_2$ layer, which diffuses outward to react with oxygen. As the oxidation reaches a certain stage, the SiO_2 scale formed on the surface layer effectively prevents oxygen from continuing to diffuse inward due to its glassy state at high-temperatures, which is continuously and densely wrapped on the surface of the coating. The key to the oxidation resistance of the silicide coating is that sufficient Si in the coating is preferentially oxidized. After long term oxidation, as shown in Fig. 11c, a low-silicide $(NbMoTaW)_5Si_3$ layer will inevitably appear at the interface between the coating and the substrate, which will weaken the oxidation resistance of the disilicide layer to a certain extent. It is worth noting that the WSi_2-rich phase precipitated in the oxidation process of the high-entropy silicide $(NbMoTaW)Si_2$ coating can slow down the formation of low silicide $(NbMoTaW)_5Si_3$, which is beneficial to improve the oxidation resistance of the coating.

Table 4
EDS composition analysis of different areas of the coating after oxidation (corresponding with Fig. 10b).

Point	Atomic percent %						
	Si	O	Nb	Mo	Ta	W	Total
1	34.32	65.68	–	–	–	–	100.0
2	36.40	60.34	–	–	1.73	1.54	100.0
3	66.70	–	7.02	7.48	9.40	9.40	100.0
4	66.92	–	10.16	8.05	8.16	6.72	100.0
5	64.30	–	8.25	8.16	9.71	9.58	100.0
6	38.83	–	13.6	13.05	16.40	18.27	100.0

4. Conclusion

A novel high-entropy silicide $(NbMoTaW)Si_2$ coating was successfully fabricated in situ on the surface of NbMoTaW alloy by the HAPC technique. Compared with pure metals, high-entropy alloys have larger lattice distortion and more vacancies, which provide more channels for Si diffusion. Therefore, the diffusion coefficient and activation energy of Si in high-entropy NbMoTaW alloys are the largest. When reaction diffusion occurs, the sluggish diffusion effect of the high-entropy alloy makes it maintain a solid solution structure, thereby promoting the formation of single-phase high-entropy $(NbMoTaW)Si_2$ with a hexagonal structure.

In the atmospheric environment of 1300 ℃, the $(NbMoTaW)Si_2$ coating specimen exhibits excellent oxidation resistance compared with the NbMoTaW alloy substrate. The oxidation resistance mechanism of

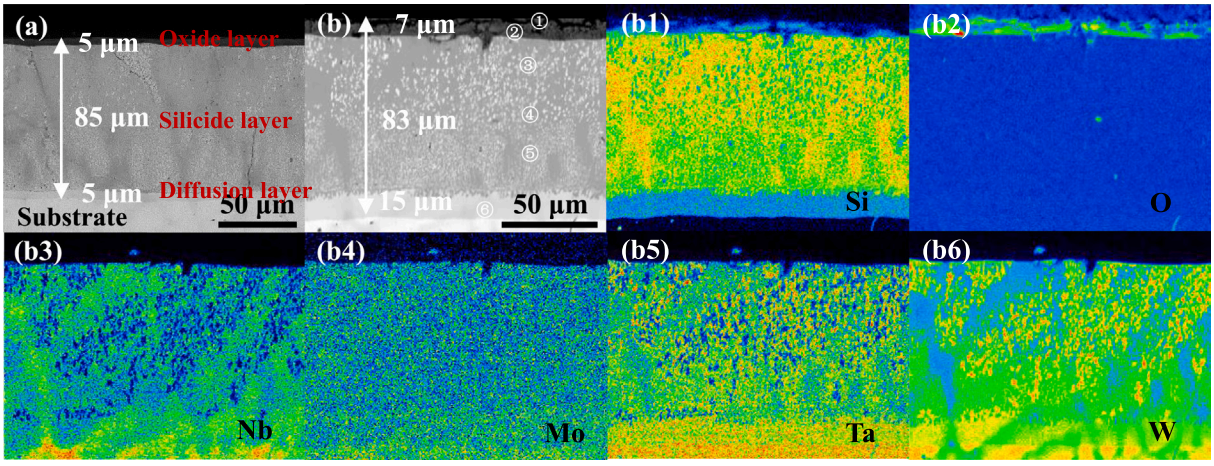

Fig. 10. Cross-section BSE images of $(NbMoTaW)Si_2$ coating specimen after oxidation at 1300 ℃ for: (a) 1 h and (b) 24 h; (b1–6): EPMA maps of (b).

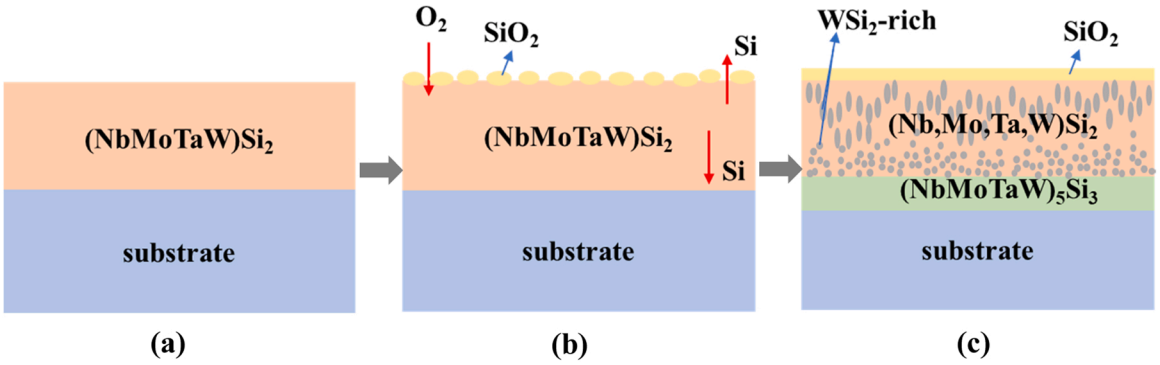

Fig. 11. Schematic diagram of oxidation behavior for (NbMoTaW)Si_2 coating specimen at 1300 ℃.

the (NbMoTaW)Si_2 coating is that a dense continuous SiO_2 oxide scale forms rapidly to restrict the inward diffusion of oxygen effectively. Moreover, the high-entropy silicide (NbMoTaW)Si_2 undergoes phase decomposition during the oxidation process to precipitate WSi_2, which can inhibit the interdiffusion of the silicide layer and the alloy substrate.

CRediT authorship contribution statement

Juan Kuang: Methodology, Data curation, Investigation, Writing – original draft. **Ping Zhang:** Investigation, Writing – review & editing. **Qianqian Wang:** Writing – review & editing. **Zhenfeng Hu:** Investigation. **Xiubing Liang:** Resources. **Baolong Shen:** Conceptualization, Funding acquisition, Project administration, Supervision, Writing – review & editing.

Declaration of Competing Interest

The authors declare that they have no known competing financial interests or personal relationships that could have appeared to influence the work reported in this paper.

Acknowledgement

This work is supported by the National Natural Science Foundation of China (Grant number 51631003).

References

[1] J.W. Yeh, S.K. Chen, S.J. Lin, J.Y. Gan, T.S. Chin, T.T. Shun, C.H. Tsau, S.Y. Chang, Nanostructured high-entropy alloys with multiple principal elements: Novel alloy design concepts and outcomes, Adv. Eng. Mater. 6 (2004) 299–303.
[2] E.P. George, D. Raabe, R.O. Ritchie, High-entropy alloys, Nat. Rev. Mater. 4 (2019) 515–534.
[3] K.Y. Tsai, M.H. Tsai, J.W. Yeh, Sluggish diffusion in Co–Cr–Fe–Mn–Ni high-entropy alloys, Acta Mater. 61 (2013) 4887–4897.
[4] D.B. Miracle, O.N. Senkov, A critical review of high entropy alloys and related concepts, Acta Mater. 122 (2017) 448–511.
[5] O.N. Senkov, D.B. Miracle, K.J. Chaput, J.P. Couzinie, Development and exploration of refractory high entropy alloys—a review, J. Mater. Res. 33 (2018) 3092–3128.
[6] O.N. Senkov, S. Gorsse, D.B. Miracle, High temperature strength of refractory complex concentrated alloys, Acta Mater. 175 (2019) 394–405.
[7] Y. Chen, Z. Xu, M. Wang, Y. Li, C. Wu, Y. Yang, A single-phase $V_{0.5}Nb_{0.5}ZrTi$ refractory high-entropy alloy with outstanding tensile properties, Mater. Sci. Eng., A 792 (2020), 139774.
[8] O.N. Senkov, G.B. Wilks, D.B. Miracle, C.P. Chuang, P.K. Liaw, Refractory high-entropy alloys, Intermetallics 18 (2010) 1758–1765.
[9] O.N. Senkov, G.B. Wilks, J.M. Scott, D.B. Miracle, Mechanical properties of $Nb_{25}Mo_{25}Ta_{25}W_{25}$ and $V_{20}Nb_{20}Mo_{20}Ta_{20}W_{20}$ refractory high entropy alloys, Intermetallics 19 (2011) 698–706.
[10] S. Sheikh, L. Gan, T.K. Tsao, H. Murakami, S. Shafeie, S. Guo, Aluminizing for enhanced oxidation resistance of ductile refractory high-entropy alloys, Intermetallics 103 (2018) 40–51.
[11] B. Gorr, S. Schellert, F. Müller, H.J. Christ, A. Kauffmann, M. Heilmaier, Current status of research on the oxidation behavior of refractory high entropy alloys, Adv. Eng. Mater. 23 (2021), 2001047.
[12] J. Sun, Q.G. Fu, L.P. Guo, L. Wang, Silicide coating fabricated by HAPC/SAPS combination to protect niobium alloy from oxidation, ACS Appl. Mater. Interfaces 8 (2016) 15838–15847.
[13] J.S. Han, B. Su, J.H. Meng, A.J. Zhang, Y.Z. Wu, Microstructure and composition evolution of a fused slurry silicide coating on MoNbTaTiW refractory high-entropy alloy in high-temperature oxidation environment, Materials 13 (2020) 3592.
[14] J.H. He, X.P. Guo, Y.Q. Qiao, F. Luo, A novel Zr-Y modified silicide coating on Nb-Si based alloys as protection against oxidation and hot corrosion, Corros. Sci. 177 (2020), 108948.
[15] R.R. Su, H.L. Zhang, G.Y. Ouyang, L.F. Liu, W. Nachlas, J. Cui, D.D. Johnson, J. H. Perepezko, Enhanced oxidation resistance of $(Mo_{95}W_5)_{85}Ta_{10}(TiZr)_5$ refractory multi-principal element alloy up to 1300 °C, Acta Mater. 215 (2021), 117114.
[16] K. Choi, W. Yang, K.H. Baik, Y. Kim, S. Lee, S. Lee, J.S. Park, Growth kinetics and isothermal oxidation behavior of a Si pack cementation-coated Mo-Si-B alloy, Appl. Surf. Sci. 489 (2019) 668–676.
[17] W. Yang, K. Choi, C. Choi, J.S. Park, Degradation properties of refractory MoNbTaVW high-Entropy alloys with simultaneous Si/Al pack cementation coatings under high-temperature flame tests, Oxid. Met. 96 (2021) 557–569.
[18] A.L. Vyatskikh, B.E. MacDonald, A.D. Dupuy, E.J. Lavernia, J.M. Schoenung, H. Hahn, High entropy silicides: CALPHAD-guided prediction and thin film fabrication, Scr. Mater. 201 (2021), 113914.
[19] D. Liu, Y.A. Huang, L. Liu, L.Q. Zhang, A novel of MSi_2 high-entropy silicide: Be expected to improve mechanical properties of $MoSi_2$, Mater. Lett. 268 (2020), 127629.
[20] J. Gild, J. Braun, K. Kaufmann, E. Marin, T. Harrington, P. Hopkins, K. Vecchio, J. Luo, A high-entropy silicide: $(Mo_{0.2}Nb_{0.2}Ta_{0.2}Ti_{0.2}W_{0.2})Si_2$, J. Mater. 5 (2019) 337–343.
[21] W.M. Choi, Y.H. Jo, S.S. Sohn, S. Lee, B.J. Lee, Understanding the physical metallurgy of the CoCrFeMnNi high-entropy alloy: an atomistic simulation study, npj Comput. Mater. 4 (2018) 1.
[22] C.C. Wang, K.Z. Li, D.Y. He, X.H. Shi, Evolution behavior of rare-earth yttria modified silicide oxidation-resistant coating at 1700 ℃, J. Eur. Ceram. Soc. 40 (2020) 4419–4427.
[23] B.V. Cockeram, R.A. Rapp, The kinetics of multilayered titanium-silicide Coatings grown by the pack cementation method, Metall. Mater. Trans. A 26 (1995) 777–791.
[24] B. Paul, J. Kishor, S. Majumdar, V. Kain, Studies on growth mechanism of intermediate layer of $(Mo,W)_5Si_3$ and interdiffusion in the (Mo,W)-$(Mo,W)Si_2$ system prepared by pack cementation coating, Surf. Interfaces 18 (2020), 100458.
[25] D. Hu, Q.G. Fu, L. Zhou, B. Liu, C.Y. Cheng, X.X. Li, J. Sun, Self-healing improvement strategy of thermally sprayed $MoSi_2$ coating at 1773 K: From calculation to experiment, Corros. Sci. 189 (2021), 109599.
[26] G. Yue, X.P. Guo, Y.Q. Qiao, Study on the diffusion barrier effect of WSi_2 layer at the $MoSi_2$/Nb-Ti-Si based alloy interface, Corros. Sci. 163 (2020), 108299.
[27] V.I. Zmii, N.V. Kovtun, P.I. Glushko, S.G. Ruden'kii, Stability and heat resistance of silicide coatings on refractory metals. II. stability and heat resistance of silicide coatings on tungsten and molybdenum at 1500–2000 ℃, Powder Metall. Met. Ceram. 42 (2003) 50–53.